Journal Pre-proofs

Tuning the electronic, photocatalytic and optical properties of hydrogenated InN monolayer by biaxial strain and electric field

Khang D. Pham, Tuan V. Vu, Tri Nhut Pham, Dat D. Vo, Phuc Toan Dang, D.M. Hoat, Chuong V. Nguyen, Huynh V. Phuc, Le T. N. Tu, Lanh Chu Van, Hien D. Tong, Nguyen T.T. Binh, Nguyen N. Hieu

Tuning the electronic, photocatalytic and optical properties of hydrogenated InN monolayer by biaxial strain and electric field

Khang D. Pham [a,b], Tuan V. Vu [c,d,*], Tri Nhut Pham [e], Dat D. Vo [c,d],

Phuc Toan Dang [c,d], D. M. Hoat [f,b], Chuong V. Nguyen [g],

Huynh V. Phuc [h], Le T. N. Tu [h], Lanh Chu Van [i], Hien D. Tong [j],

Nguyen T.T. Binh [k,*], Nguyen N. Hieu [k,*]

[a]*Laboratory of Applied Physics, Advanced Institute of Materials Science, Ton Duc Thang University, Ho Chi Minh City, Viet Nam*

[b]*Faculty of Applied Sciences, Ton Duc Thang University, Ho Chi Minh City, VietNam*

[c]*Institute for Computational Science, Ton Duc Thang University, Ho Chi Minh City, Viet Nam*

[d]*Faculty of Electrical & Electronics Engineering, Ton Duc Thang University, Ho Chi Minh City, Viet Nam*

[e]*Center of Excellence for Green Energy and Environmental Nanomaterials, Nguyen Tat Thanh University, Ho Chi Minh City, Viet Nam*

[f]*Computational Laboratory for Advanced Materials and Structures, Advanced Institute of Materials Science, Ton Duc Thang University, Ho Chi Minh City, Viet Nam*

[g]*Department of Materials Science & Engineering, Le Quy Don Technical University, Ha Noi, Viet Nam*

[h]*Division of Theoretical Physics, Dong Thap University, Cao Lanh, Viet Nam*

[i]*Department of Physics, Vinh University, 182 Le Duan, Vinh City, Viet Nam*

[j]*Faculty of Engineering, Vietnamese-German University, Binh Duong, Viet Nam*

[k]*Institute of Research and Development, Duy Tan University, Da Nang 550000, Viet Nam*

Abstract

We investigate the electronic, photocatalytic and optical properties of a fully hydrogenated indium nitride H–InN–H monolayer under biaxial strain ε_b and external electric field E using density functional theory. Our findings demonstrate that the H–InN–H monolayer is a semiconductor with an indirect energy gap of 2.591 eV. Under a biaxial strain or electric field, the indirect–direct band gap transition can occur and its band gap depends dramatically on the ε_b and E. Our analysis of band edge alignment shows that the H–InN–H monolayer can possess photocatalytic activity for water splitting when an electric field or biaxial strain is applied. The optical characteristics of the H–InN–H monolayer depends greatly on the strain. The first optical gap of the H–InN–H monolayer is at the incident energy light of 3.320 eV and the tensile strain causes the first optical gap to shift towards the visible light region.

Key words: Monolayer InN, surface hydrogenation, electronic and optical properties, photocatalytic activity, density functional theory

* Corresponding authors.
  Email addresses: phamdinhkhang@tdtu.edu.vn (Khang D. Pham),
vuvantuan@tdtu.edu.vn (Tuan V. Vu),
nguyentthanhbinh8@duytan.edu.vn (Nguyen T.T. Binh),
hieunn@duytan.edu.vn (Nguyen N. Hieu).

1 Introduction

Since the successful mechanical exfoliation, graphene has become one of the materials that scientists are of prime interest [1]. Graphene has created a profound revolution in nanoelectronic technologies and many new-generation devices based on graphene with outstanding functions have been built [2]. However, in the semimetal form with zero band gap band, graphene has certain limitations in its application to optoelectronic devices [3]. In parallel with finding a way to overcome this drawback in graphene [4, 5], scientists have looked for other two-dimensional (2D) layered graphene-like materials [6–10]. These materials, especially binary compounds, have shown great potential applications in nanoelectronic devices and photocatalytic water splitting [11–16]. The group-III nitride monolayers such as InN or GaN are semiconductors with many promising applications in technology [17]. In particular, with the ability to high-speed data transfer [18], InN is expected to be a material with many applications in new-generation devices.

The InN thin-films have been successfully synthesized recently by the metal-organic chemical vapor deposition [19] and the plasma-assisted molecular beam epitaxy [20]. Previously, the surface-functionalization of InN has been studied experimentally [21]. In the monolayer form, InN is a semiconductor with band gap from 0.6 eV to 0.8 eV [17, 22, 23]. Based on the analysis of the phonon spectrum, one has confirmed that the InN monolayer is dynamically stable at equilibrium [22, 24]. Prete and co-workers have demonstrated that the InN monolayer is an excellent candidate for applications in optoelectronic devices due to its outstanding optical properties [23, 25]. Similar to graphene or other layered two-dimensional (2D) materials, electronic and transport properties of InN monolayer depend greatly on the strain or applied pressure [26]. Recently, one of the ways to modify the physical properties of 2D materials is using the chemically surface-functionalization [27,

3

28]. Lin and co-workers has demonstrated that the surface-functionalization of group III monochalcogenide monolayers with hydrogen is a significant change in their electronic properties, especially the increase in their band gap to satisfy the requirements for possesses photocatalytic activity for water splitting in these monolayers [29]. Previously, modification of electronic properties of GaN and related binary compound monolayers by chemical functionalization has been studied by ab-initio calculations [30, 31]. Using first-principles calculations, Vu and co-workers have demonstrated that surface-functionalization not only alters the band alignment of the GeC monolayer, but also significantly changes its optical properties, in particular it greatly alters the absorption characteristics of the monolayer [32, 33].

In this work, we systematically consider the electronic, photocatalytic and optical properties of a fully hydrogenated indium nitride H–InN–H using density functional theory. Influence of a biaxial strain ε_b and external electric field E on the electronic, photocatalytic and optical properties of the H–InN–H monolayer is also studied. We focus on the modification of the band structures, photocatalytic activity for water splitting and basic optical characteristics of the H–InN–H monolayer in the presence of the ε_b and electric field E.

2 Computational method

In the present study, we perform all calculations for the pristine InN and fully hydrogenated indium nitride H–InN–H monolayers based on density functional theory (DFT) using the Quantum Espresso package [34]. We use the generalized gradient approximation (GGA) by Perdew-Burke-Ernzerhof (PBE) [35, 36]. Besides, to correctly treat the weak van der Waals interactions which may exist in the layered material, we use also the Grimme's semi-empirical DFT-D2 method [37]. For a plane-wave basis, the energy cut-off is set to be 500 eV. In the Brillouin

4

zone, a $(15 \times 15 \times 1)$ k-mesh is used for calculations of electronic properties of the pristine InN and fully hydrogenated indium nitride H–InN–H monolayers. The structures of monolayers were fully optimized with the criteria for force and energy convergence is 10^{-3} eV/Å and 10^{-6} eV, respectively. A supercell (4×4) for the InN monolayer was built for the calculations. To avoid any interaction that might exist between neighbor slabs, a perpendicularly vacuum space of 20 Å to the 2D surface of the monolayers was used in our calculations.

To consider the effect of biaxial strain on physical properties of monolayers, we define the biaxial strain ε_b via the lattice parameters before $\mathcal{L}_0$ and after strain $\mathcal{L}$ of the H–InN–H monolayer as $\varepsilon_b = (\mathcal{L} - \mathcal{L}_0)/\mathcal{L}_0$. In this work, a biaxial strain from -10% to 10% is applied to the H–InN–H monolayer. The minus and plus signs refer to the compressive and tensile biaxial strains, respectively. Besides, We have applied electric field perpendicular to the H–InN–H monolayer 2D surface to investigate its effect on the electronic, photocatalytic and optical properties of the H–InN–H monolayer.
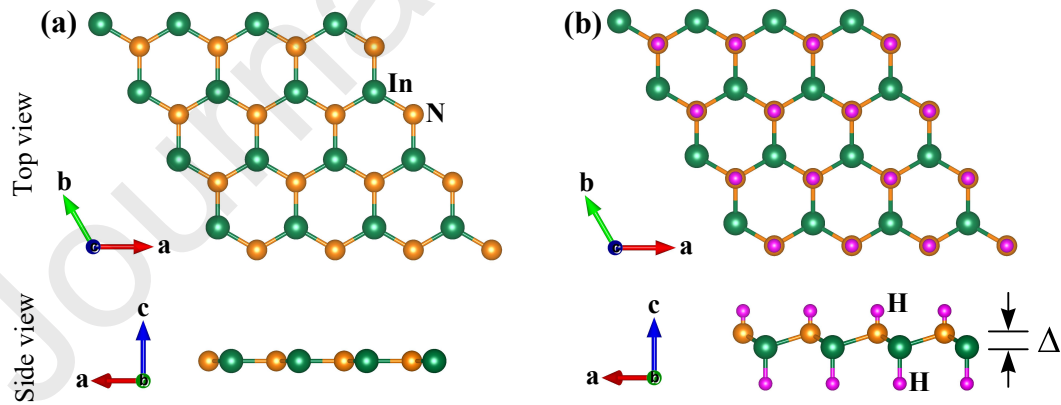
Fig. 1. Top ans side views of atomic structure after relaxation of monolayers (a) pristine InN and (b) fully hydrogenated indium nitride H–InN–H at equilibrium. **a**, **b**, **c** are the coordinate axes.

3 Results and discussion

Monolayer InN is a compound consisted of the In and N atoms which arranged in the hexagonal lattice. At equilibrium, monolayer InN is in the planar structure with the lattice parameter of 3.616 Å. Our obtained result is consistent with the previous DFT studies [17, 22, 25]. Due to the surface-functionalization by hydrogen atoms, the planar structure of InN monolayer is broken and fully hydrogenated indium nitride monolayer H–InN–H has a low-bucked structure with bucking constant of $\Delta = 0.639$ Å. The optimized atomic structures of the InN and H–InN–H monolayers at equilibrium are depicted in Fig. 1. Our calculated results also indicate that the structure of monolayer InN is significantly changed upon the surface-functionalization by hydrogen atoms. The lattice parameter of the H–InN–H is $a = 3.590$ Å which is smaller than that of the pristine InN monolayer. The thickness of the H–InN–H monolayer (distance between two hydrogen layers) is 3.365 Å. However, in the H–InN–H monolayer, the difference in bond lengths between H atoms and N/In atoms are quite large, $d_{\text{H–In}} = 1.688$ Å and $d_{\text{H–N}} = 1.038$ Å. The structural parameters of both pristine InN and H–InN–H monolayers are also listed in Tab. 1. The binding energy E_b is calculated via the following expression:

$$E_b = E_{\text{tot}} - n_a E_{\text{In}} - n_b E_{\text{N}} - n_c E_{\text{H}}, \tag{1}$$

where E_{tot} is the total energy of the InN monolayer, E_{In}, E_{N}, and E_{H} are the total energies of the In, N, and H atoms, respectively. n_a, n_b, and n_c are the numbers of the In, N, and H atoms in the computed cells, respectively. The obtained results for the binding energies of the pristine InN and fully hydrogenated InN monolayers are -12.126 eV and -19.746 eV, respectively. All the binding energies are negative that implies that the binding between atoms in these systems are strong. Also, to

6

Table 1

Calculated lattice parameter a, bond lengths between atoms d, bucking constant Δ, thickness (Å), binding energy E_b (eV), and band gap (eV) of pristine InN and H–InN–H monolayers at equilibrium.

	a	$d_{\text{In–N}}$	$d_{\text{In–H}}$	$d_{\text{N–H}}$	Δ	Thickness	E_b	Band gap
InN	3.616	2.088	-	-	-	-	-12.126	0.712
H–InN–H	3.590	2.169	1.688	1.038	0.639	3.365	-19.746	2.591
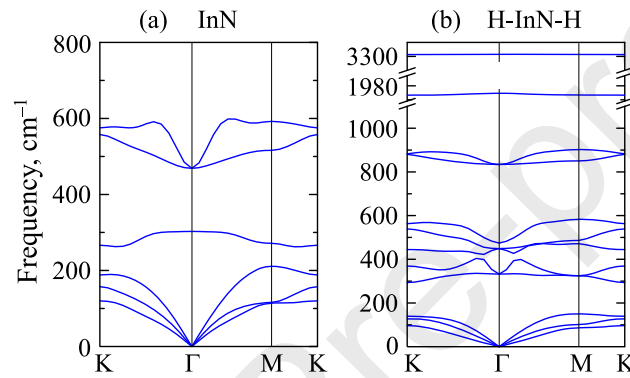
Fig. 2. Phonon dispersion curves of (a) InN and (b) fully hydrogenated indium nitride H–InN–H monolayers at equilibrium.

check the dynamically stability of the monolayers, we perform the calculations for the phonon dispersion curves of the pristine InN and H–InN–H monolayers. As shown in Fig. 2, we can see that there are no soft phonon modes in the phonon dispersion curves of these monolayers. This implies that both the pristine InN and H–InN–H monolayers are dynamically stable at equilibrium.

At equilibrium, our DFT calculations indicate that both the pristine InN and H–InN–H monolayers are indirect-gap semiconductors. The calculated energy gap of the pristine InN and H–InN–H monolayers are 0.712 eV and 2.591 eV respectively. Obviously, the surface-functionalization leads to significantly increase the band gap of the monolayer InN. It is well-known that the GGA-PBE functional un-

7
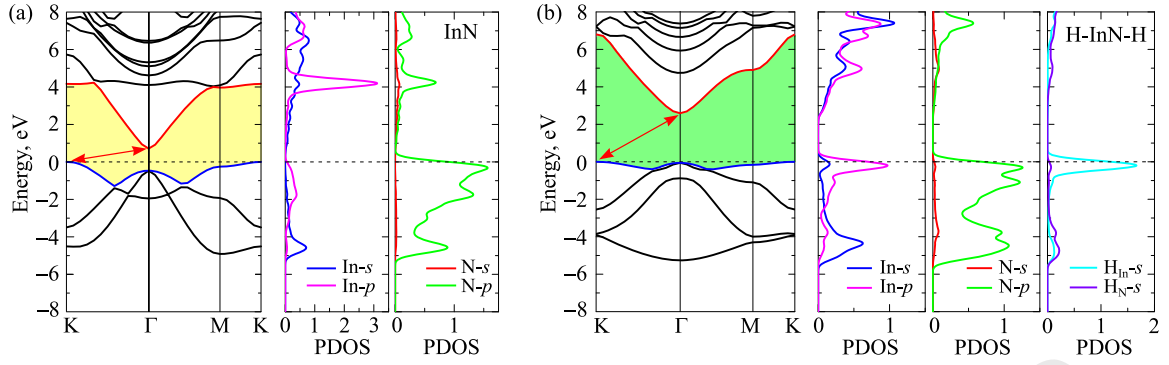
Fig. 3. Band structure and PDOS of (a) InN and (b) H–InN–H monolayers at equilibrium.

derestimates the band gap of the semiconductors [38] and some corrections, such as the Heyd–Scuseria–Ernzerhof (HSE06) hybrid functional [39] or GW method [40], have been suggested. However, the calculated band structure of monolayer at the GGA-PBE and HSE06 levels are the same profile. The basic characteristics of the electronic properties of the monolayers are unchanged whether they are calculated by GGA-PBE and HSE06 functionals. Band structures and partial density of states of the InN and H–InN–H monolayers are shown in Fig. 3. The band structures are plotted along the K-Γ-M-K high-symmetry direction in the range of energy from -8 eV to 8 eV. We can see that, in both monolayers, the conduction band minimum (CBM) and the valence band maximum (VBM) are located at the Γ- and K-point, respectively. Looking inside the band structure of the H–InN–H monolayer, we realize that even though the VBM located at the K-point, however the energy difference between the highest energies of the valence band at the K-point and Γ-point is very small. This point can suggest that we can modulate the band structure of the H–InN–H by external conditions such as electric field or strain engineering and we can expect that indirect-direct band gap transition will occur in the presence of strain or electric field. To better see the contribution of the orbitals of atoms to the formation of electronic bands, we also calculated the partial density of states (PDOS) as illustrated in Fig. 3. In the case of the H–InN–H as shown in Fig. 3(b),

8

we see that the valence band of the H–InN–H monolayer is mainly contributed by the N-p orbitals. In the energy region from -6 eV to 0 eV, the contribution of the N-p orbitals to the valence band is markedly superior to that from other orbitals. Besides, the valence band near the Fermi level is significantly contributed from the In-s orbital. The In-s and In-p orbitals contribute fairly evenly to the conduction band at the high energy domain of from 5 eV to 8 eV. Our calculations indicate that, while the contribution of the H_{In}-s orbitals of the H atom on the In side to the bands of the H–InN–H monolayer is significant in a small range of energy near the Fermi level, the contributions of the s-orbitals from H atoms from both sides, i.e., H_{In}-s and H_N-s orbitals, to both the valence and conduction bands is quite small.

It is well-known that the layered materials are sensitive particularly to structural perfection. We next investigate the influence of biaxial strain ε_b on the electronic properties of the fully hydrogenated indium nitride H–InN–H monolayer.
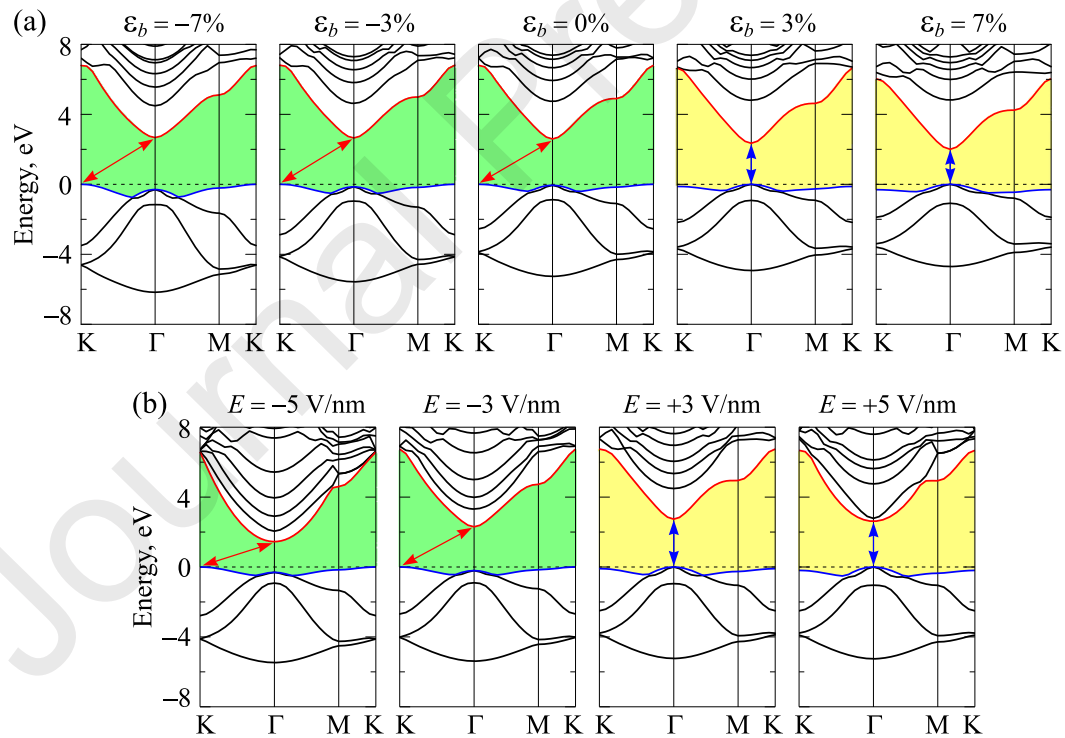
Fig. 4. Band structures of the H–InN–H monolayer under different levels of the ε_b (a) and the E (b).

The calculated band structures of the H–InN–H monolayer under different levels of the ε_b are depicted in Fig. 4(a). We can see that, the influence of the strain engineering ε_b on the band structure of the fully hydrogenated indium nitride H–InN–H monolayer is significant, particularly in the tensile strain case $\varepsilon_b > 0$. When the tensile biaxial strain was introduced, as above-predicted, the VBM of the H–InN–H monolayer has moved from the K- to Γ-point and the H–InN–H monolayer becomes a direct semiconductor. It means that the tensile biaxial strain leads to the indirect–direct energy gap transition in the fully hydrogenated indium nitride monolayer. Contrary to the case of tensile strain, the influence of compression strain on the band structure of the fully hydrogenated indium nitride monolayer is quite weak. Under the compression strain, the fully hydrogenated indium nitride H–InN–H monolayer is still the indirect semiconductor and the energy gap of the fully hydrogenated indium nitride monolayer is changed insignificantly due to the compression biaxial strain as shown in Fig. 5(a). In the presence of compression biaxial strain from 0 to -10%, the energy gap of the H–InN–H tends to increase slightly then decrease. However, the decrease is not significant. The maximum band gap is 2.678 eV at the $\varepsilon_b = -5\%$ compared to 2.591 eV at equilibrium $\varepsilon_b = 0\%$. Also, from Fig. 5(a) we can conclude that the tensile strain not only leads to indirect–direct band gap transition but also quickly reduces the energy gap of the H–InN–H monolayer. In the tensile case $\varepsilon_b > 0$, the change tendency of the energy gap is quite obvious. The energy gap of the H–InN–H monolayer decreases linearly with the tensile strain.

Similar to the case of the H–InN–H under strain engineering, the electronic properties of the H–InN–H monolayer depend quite strongly on the external electric field E, especially when the intensity of the electric field is quite large. To investigate the influence of the E on the electronic properties of the H–InN–H monolayer, an electric field is applied perpendicularly to the 2D surface of the fully

10
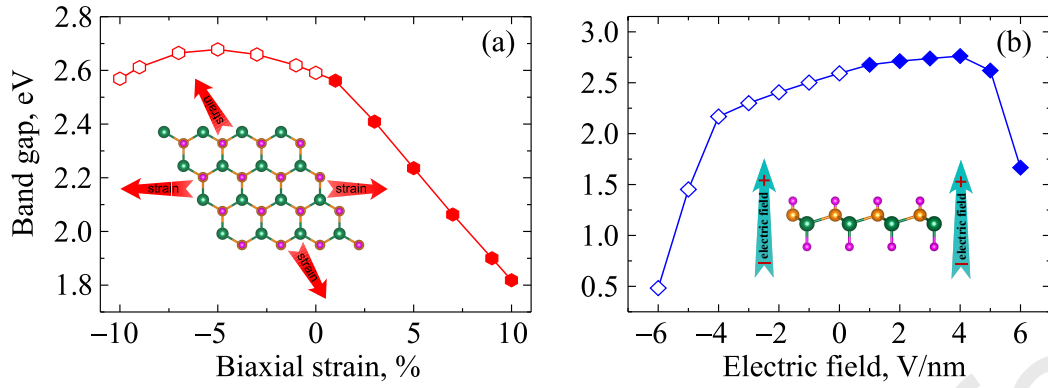
Fig. 5. Band gap of the H–InN–H monolayer as a function of the biaxial strain (a) and the electric field (b). Unfilled and filled symbols refer to the indirect and direct band gaps, respectively.

hydrogenated indium nitride monolayer and the direction of the electric field is along the c-direction. In this work, a large range of the E from -6 V/nm to 6 V/nm is applied to the system. Band structures of the H–InN–H monolayer in the presence of the external electric field E are shown in Fig. 4(b). Our DFT calculations demonstrate that the negative E did not change the characteristics of the forbidden band of the H–InN–H monolayer, that is, the H–InN–H monolayer is still an indirect semiconductor under the negative field. In the case of the positive electric field, the position of the VBM is moved from the K- to Γ-point while the CBM remains at the Γ-point. It means that the indirect–direct gap transition has occurred and the H–InN–H monolayer becomes a direct semiconductor when placed in an electric field oriented along the positive direction of the c-axis. The obtained results demonstrate that in the E varying from -4 to 4 V/nm, the influence of the electric field on the band gap is quite weak. The energy gap of the H–InN–H monolayer at $E = -4$ V/nm and $E = 4$ V/nm are 2.167 eV and 2.761 eV, respectively. This value is not much different from the band gap at the equilibrium state (2.591 eV). However, as the intensity of the E continues to increase, band gap of the H–InN–H monolayer quite quickly decreases as shown in Fig. 5(b).

11

It is well-known that the standard oxidation and potentials are dependent on the pH value [41]. The standard oxidation potential O_2/H_2O at the $pH = 0$ is 1.23 eV vs. the normal hydrogen electrode (NHE) or -5.67 eV vs. the vacuum level and the standard hydrogen reduction potential of the H^+/H_2 is 0 eV vs. the NHE or -4.44 eV vs. the vacuum level. The condition for the material possessing the photocatalytic activity is the conduction band minimum (CBM) must be more negative than the standard hydrogen reduction potential of the H^+/H_2 (0 eV) and the valence band maximum (VBM) must be more positive than the oxidation potential O_2/H_2O (1.23 eV). Also, because the standard oxidation potential O_2/H_2O is 1.23 eV vs. the NHE, therefore the energy gap required for photocatalysts must be bigger than 1.23 eV. As above-mentioned, the energy gap of the monolayer H–InN–H at equilibrium is 2.591 eV. Therefore, the H–InN–H monolayer is capable of possessing photocatalytic properties. We will examine the photocatalytic properties for water splitting of the H–InN–H monolayer and the effect of strain ε_b and electric field on its photocatalytic activity through calculations for the CBM and VBM edge alignment. Our DFT findings demonstrate that at the equilibrium state, the positions of the CBM and VBM are located at 0.022 eV and 2.613 eV, respectively. It means that the H–InN–H monolayer at the equilibrium state does not possess the photocatalytic activity for water splitting. However, because the position of the VBM is much more positive than the standard oxidation potential O_2/H_2O. This means that the ability to possess the photocatalytic activities for water splitting depends greatly on the location of the CBM. If the external conditions such as ε_b or E can shift the CBM position towards the negative side of the standard oxidation potential, the H–InN–H monolayer will possess photocatalytic activity for water splitting. The VBM and CBM edge alignment of the H–InN–H monolayer under the ε_b and E is illustrated in Fig. 6. From Fig. 6(a), we can see that when the ε_b is applied, the fully hydrogenated indium nitride H–InN–H monolayer possesses photocatalytic activ-
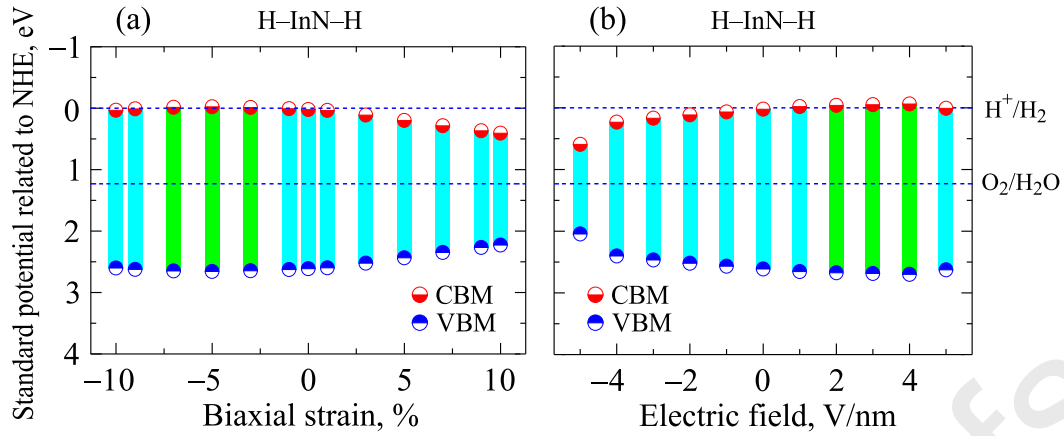
Fig. 6. Band alignment. The CBM and VBM edge alignment of the H–InN–H monolayer under biaxial strain (a) and electric field (b). The standard hydrogen reduction and oxidation potentials for water splitting at the $pH = 0$ are indicated by the horizontal dashed lines.

ity for water splitting in a quite large range of the ε_b from -7% to -3%. Focusing on the calculated results for the CBM and VBM edge alignment of the H–InN–H monolayer under external electric field in Fig. 5, we can see that the electric field E can also tune the photocatalytic properties in the H–InN–H monolayer. Under the applied E varying from 2 V/nm to 4 V/nm, the H–InN–H monolayer posses the photocatalytic activity for water splitting with the CBM located at a slightly negative position than the standard oxidation potential.

We next investigate the optical characteristics of the fully hydrogenated indium nitride H–InN–H under the ε_b and E. We concentrate only on the basic characteristics such as dielectric function $\varepsilon(\omega)$ and the absorption coefficient $\alpha(\omega)$ of the H–InN–H monolayer. In this work, the incident light is polarized along the a-axis (parallel polarization) with the energy of photon in the range from 0 to 20 eV. The dielectric function $\varepsilon(\omega)$ is given by

$$\varepsilon(\omega) = \varepsilon_1(\omega) + i\varepsilon_2(\omega), \tag{2}$$

where $\varepsilon_2(\omega)$ is the imaginary part of the $\varepsilon(\omega)$ which is calculated by sum of the transitions between occupied–unoccupied states and the real part $\varepsilon_1(\omega)$ can be es-

timated through the Kramer-Kronig transformation. The $\varepsilon_2(\omega)$ is given by [42, 43]

$$\varepsilon_2^{ij}(\omega) = \frac{Ve^2}{2\pi\hbar m^2\omega^2} \int d^3\mathbf{k} \sum_{nn'} \langle \mathbf{k}n \,|p_i|\, \mathbf{k}n' \rangle \langle \mathbf{k}n' \,|p_j|\, \mathbf{k}n \rangle$$
$$\times f_{\mathbf{k}n}(1 - f_{\mathbf{k}n'})\delta(E_{\mathbf{k}n'} - E_{\mathbf{k}n} - \hbar\omega), \qquad (3)$$

where m and e are respectively the mass and charge of the electron, ω is the electromagnetic irradiation frequency, $\mathbf{p}$ is the momentum operator, $\mathbf{k}$ is the wavevector, $|\mathbf{k}n\rangle$ part stands for the crystal wave-function regarding to energy $E_{\mathbf{k}n}$, and $f_{\mathbf{k}n}$ is the function of the Fermi distribution.

In Fig. 7, we show the parts of the dielectric function of the H–InN–H monolayer as function of the ε_b and E. Our obtained results indicate that the first optical gap of the H–InN–H monolayer is at the incident energy light of 3.320 eV. This energy value corresponds to the boundary between the visible light and ultraviolet light. Focusing on the effect of the strain ε_b on optical characteristics of the H–
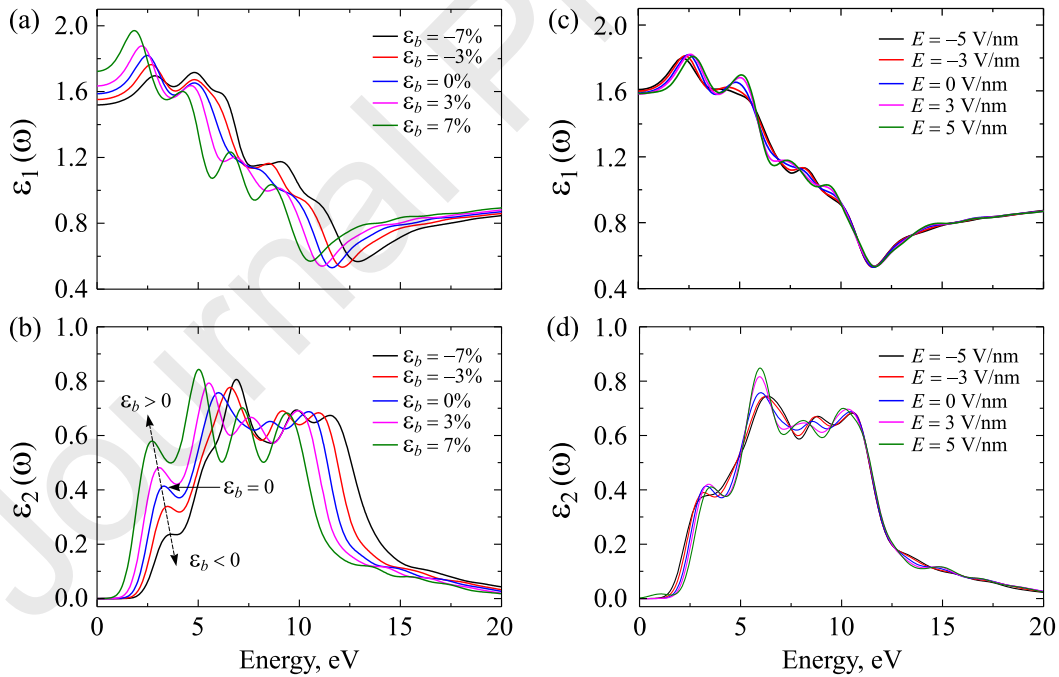
Fig. 7. Calculated parts of dielectric functions of the H–InN–H monolayer under biaxial strain ε_b (a,b) and external electric field (c,d).

InN–H monolayer, we realize that, as shown in Fig. 7(b), the tensile strain causes the first optical gap to shift towards the lower energy region (shift to the visible light region) while the first optical gap is shifted to the higher energy domain in the presence of the compressive strain $\varepsilon_b < 0$. Unlike the case of strain engineering, the influence of the external electric field E on the parts $\varepsilon_1(\omega)$ and $\varepsilon_2(\omega)$ of the dielectric constant is quite weak as shown in Fig. 7(c,d). This is also consistent with the previous results for other surface-functionalized 2D materials that the effect of electric fields on their optical properties is very weak [32, 33].

The absorption coefficient $\alpha(\omega)$ is defined through the $\varepsilon(\omega)$ function which is given by [43, 44]

$$\alpha(\omega) = \frac{\sqrt{2}\omega}{c} \left[\sqrt{\varepsilon_1^2(\omega) + \varepsilon_2^2(\omega)} - \varepsilon_1(\omega) \right]^{1/2}. \qquad (4)$$

In Fig. 8, we illustrate the obtained results for the $\alpha(\omega)$ of the H–InN–H monolayer under the ε_b and E. At the equilibrium state, the maximum of the absorption coefficient is $\alpha(\omega)_{\max} = 6.377 \times 10^4$ cm^{-1} at 10.929 eV. Obtained results demonstrate that, while the influence of the E on the absorption coefficient $\alpha(\omega)$ is negligible, the maximum of the $\alpha(\omega)$ can be increased by compressive strain.
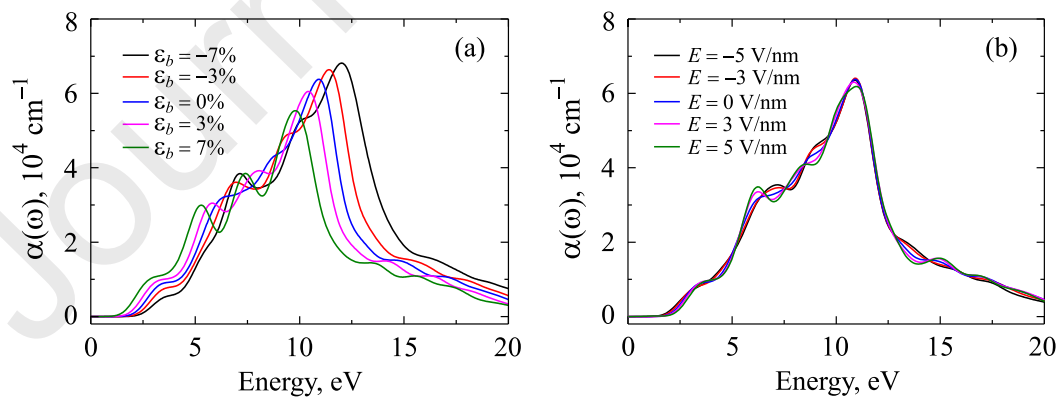
Fig. 8. Calculated $\alpha(\omega)$ of the H–InN–H monolayer under biaxial strain ε_b (a) and external electric field (b).

15

4 Conclusion

In this work, we have considered the electronic, photocatalytic and optical properties of the surface-functionalized indium nitride monolayer with hydrogen atoms H–InN–H under strain engineering and electric field by density functional theory. Our DFT calculations demonstrate that the electronic and optical properties of the H–InN–H monolayer depend greatly on the strain engineering. The shifting of the first optical gap due to the effects of biaxial strain, especially the first optical gap shifting to the visible light domain in the tensile strain case, plays an important role in the prospect of application in optoelectronic devices. Most importantly, the H–InN–H monolayer can possess photocatalytic activity for water splitting when the strain engineering or electric field when was introduced. This has opened up great perspectives on the use of the H–InN–H monolayer as a photocatalyst for applications in water-splitting technology.

References

[1] K. S. Novoselov, A. K. Geim, S. V. Morozov, D. Jiang, Y. Zhang, S. V. Dubonos, I. V. Grigorieva, A. A. Firsov, Science 306 (2004) 666.

[2] J. Yang, P. Hu, G. Yu, APL Mater. 7 (2019) 020901.

[3] F. Schwierz, Nat. Nanotechnol. 5 (2010) 487.

[4] A. K. Geim, I. V. Grigorieva, Nature 499 (2013) 419.

[5] H. V. Phuc, N. N. Hieu, B. D. Hoi, C. V. Nguyen, Phys. Chem. Chem. Phys. 20 (2018) 17899.

[6] D. Hoat, T. V. Vu, M. M. Obeid, H. R. Jappor, Chem. Phys. 527 (2019) 110499.

[7] M. M. Obeid, M. M. Shukur, S. J. Edrees, R. Khenata, M. Ghebouli, S. A. Khandy, A. Bouhemadou, H. R. Jappor, X. Wang, Chem. Phys. 526 (2019) 110414.

[8] H. R. Jappor, M. M. Obeid, T. V. Vu, D. Hoat, H. D. Bui, N. N. Hieu, S. J. Edrees, Y. Mogulkoc, R. Khenata, Superlattice Microstruct. 130 (2019) 545.

[9] M. M. Obeid, H. R. Jappor, K. Al-Marzoki, D. Hoat, T. V. Vu, S. J. Edrees, Z. M. Yaseen, M. M. Shukur, Comput. Mater. Sci. 170 (2019) 109201.

[10] N. D. Hien, N. Q. Cuong, L. M. Bui, P. C. Dinh, C. V. Nguyen, H. V. Phuc, N. V. Hieu, H. R. Jappor, L. T. Phuong, B. D. Hoi, L. C. Nhan, N. N. Hieu, Physica E 111 (2019) 201.

[11] H. T. Nguyen, T. V. Vu, N. T. Binh, D. Hoat, N. V. Hieu, N. T. Anh, C. V. Nguyen, H. V. Phuc, H. R. Jappor, M. M. Obeid, N. N. Hieu, Chem. Phys. 529 (2020) 110543.

[12] T. V. Vu, N. V. Hieu, L. T. P. Thao, N. N. Hieu, H. V. Phuc, H. D. Bui, M. Idrees, B. Amin, L. M. Duc, C. V. Nguyen, Phys. Chem. Chem. Phys. 21 (2019) 22140.

[13] H. D. Bui, H. R. Jappor, N. N. Hieu, Superlattice Microstruct. 125 (2019) 1.

[14] K. D. Pham, V. T. T. Vi, D. V. Thuan, L. T. T. Phuong, L. T. Hoa, N. V. Hieu, C. V. Nguyen, H. V. Phuc, H. R. Jappor, N. Q. Cuong, B. D. Hoi, N. N. Hieu, Mater. Res. Express 6 (2019) 115002.

[15] A. A. Attia, H. R. Jappor, Chem. Phys. Lett. 728 (2019) 124.

[16] N. A. Poklonski, S. V. Ratkevich, S. A. Vyrko, A. T. Vlassov, N. N. Hieu, Int. J. Nanosci. 18 (2019) 1940008.

[17] Y. Ota, Solid State Commun. 270 (2018) 147.

17

[18] I. Wilke, R. Ascazubi, H. Lu, W. J. Schaff, Appl. Phys. Lett. 93 (2008) 221113.

[19] K. J. Chang, J. Y. Chang, M. C. Chen, S. M. Lahn, C. J. Kao, Z. Y. Li, W. Y. Uen, G. C. Chi, J. Vac. Sci. Technol. A 25 (2007) 701.

[20] P. Chen, H. Makino, T. Yao, J. Cryst. Growth 269 (2004) 66.

[21] J. M. Zavada, R. G. Wilson, C. R. Abernathy, S. J. Pearton, Appl. Phys. Lett. 64 (1994) 2724.

[22] H. Şahin, S. Cahangirov, M. Topsakal, E. Bekaroglu, E. Aktürk, R. T. Senger, S. Ciraci, Phys. Rev. B 80 (2009) 155453.

[23] M. S. Prete, O. Pulci, F. Bechstedt, Phys. Rev. B 98 (2018) 235431.

[24] H. L. Zhuang, A. K. Singh, R. G. Hennig, Phys. Rev. B 87 (2013) 165415.

[25] M. S. Prete, A. Mosca Conte, P. Gori, F. Bechstedt, O. Pulci, Appl. Phys. Lett. 110 (2017) 012103.

[26] J. Jalilian, M. Naseri, S. Safari, M. Zarei, Physica E 83 (2016) 372.

[27] R. Ruoff, Nat. Nanotechnol. 3 (2008) 10.

[28] S. Wellnhofer, A. Stabile, D. Kochan, M. Gmitra, Y.-W. Chuang, J. Zhu, J. Fabian, Phys. Rev. B 100 (2019) 035421.

[29] J. Lin, B. Zhang, T. Zheng, J. Phys. Chem. C 123 (2019) 27697.

[30] Q. Chen, H. Hu, X. Chen, J. Wang, Appl. Phys. Lett. 98 (2011) 053102.

[31] D. M. Hoat, M. Naseri, R. Ponce-Péreze, N. N. Hieu, J. F. Rivas-Silva, T. V. Vu, H. D. Tong, G. H. Cocoletzi, Mater. Res. Express 7 (2019) 015013.

[32] T. V. Vu, N. T. T. Anh, D. P. Tran, D. Hoat, N. T. Binh, H. D. Tong, B. D. Hoi, C. V. Nguyen, H. V. Phuc, N. N. Hieu, Superlattice Microstruct. 137 (2020) 106359.

[33] T. V. Vu, N. T. T. Anh, D. Hoat, D. P. Tran, H. D. Tong, H. L. Luong, L. M. Hieu, C. V. Nguyen, H. V. Phuc, N. T. Binh, N. N. Hieu, Physica E 117 (2020) 113857.

18

[34] P. Giannozzi, S. Baroni, N. Bonini, M. Calandra, R. Car, C. Cavazzoni, D. Ceresoli, G. L. Chiarotti, M. Cococcioni, I. Dabo, A. D. Corso, S. de Gironcoli, S. Fabris, G. Fratesi, R. Gebauer, U. Gerstmann, C. Gougoussis, A. Kokalj, M. Lazzeri, L. Martin-Samos, N. Marzari, F. Mauri, R. Mazzarello, S. Paolini, A. Pasquarello, L. Paulatto, C. Sbraccia, S. Scandolo, G. Sclauzero, A. P. Seitsonen, A. Smogunov, P. Umari, R. M. Wentzcovitch, J. Phys. Condens. Matter 21 (2009) 395502.

[35] J. P. Perdew, K. Burke, M. Ernzerhof, Phys. Rev. Lett. 77 (1996) 3865.

[36] J. P. Perdew, K. Burke, M. Ernzerhof, Phys. Rev. Lett. 78 (1997) 1396.

[37] S. Grimme, J. Computat. Chem. 27 (2006) 1787.

[38] J. P. Perdew, M. Levy, Phys. Rev. Lett. 51 (1983) 1884.

[39] J. Heyd, G. E. Scuseria, M. Ernzerhof, J. Chem. Phys. 118 (2003) 8207.

[40] L. Hedin, Phys. Rev. 139 (1965) A796.

[41] K. Ren, C. Ren, Y. Luo, Y. Xu, J. Yu, W. Tang, M. Sun, Phys. Chem. Chem. Phys. 21 (2019) 9949.

[42] A. Delin, P. Ravindran, O. Eriksson, J. Wills, Int. J. Quantum Chem. 69 (1998) 349–358.

[43] S. Z. Karazhanov, P. Ravindran, A. Kjekshus, H. Fjellvag, B. G. Svensson, Phys. Rev. B 75 (2007) 155104.

[44] P. Ravindran, A. Delin, B. Johansson, O. Eriksson, J. M. Wills, Phys. Rev. B 59 (1999) 1776.